Structural alterations in lecithin-cholesterol vesicles following interactions with monomeric and micellar bile salts: physical-chemical basis for subselection of biliary lecithin species and aggregative states of biliary lipids during bile formation

David E. Cohen, Mario Angelico,[1] and Martin C. Carey[2]

Departments of Medicine, Physiology, and Biophysics, Harvard Medical School, Brigham and Women's Hospital, and Harvard Digestive Diseases Center, Boston, MA 02115

Abstract Using complementary physical-chemical methods including turbidimetry, quasielastic light scattering, gel filtration, and phase analysis, we examined the interactions between dilute concentrations of the common bile salt, taurochenodeoxycholate (TCDC), and uni- and multilamellar vesicles (MLVs) composed of defined molecular species of lecithin (L) and varying contents of cholesterol (Ch). Dissolution rates of MLVs with micellar TCDC, as assessed by turbidimetry, were more rapid with vesicles composed of *sn*-1 palmitoyl species, typical of biliary L, compared with those composed of the more hydrophobic *sn*-1 stearoyl species. Incorporation of Ch retarded MLV dissolution rates in proportion to the Ch content, and only at high Ch contents were dissolution rates appreciably influenced by the *sn*-2 fatty acid composition of L. When MLVs contained Ch in amounts characteristic of intracellular membranes (Ch/L ~0.1), the dissolution rates of the individual L species by TCDC accurately predicted the steady state L composition of human bile. TCDC interacted with small unilamellar L/Ch vesicles (SUVs) at concentrations well below, as well as appreciably above, its critical micellar concentration. In accordance with the TCDC-egg yolk L-H_2O phase diagram, perimicellar concentrations of TCDC interacted with SUVs to form aggregates that were approximately twice the size of the SUVs. These were consistent with the formation of a dispersed hexagonal (rod-like) phase, which co-existed with aqueous bile salt (BS) monomers and either micellar or unilamellar SUV phases. Micellar TCDC completely solubilized SUVs as mixed micelles, putatively via this transient hexagonal phase. With modest Ch-supersaturation, dissolution was followed by the reemergence of a new vesicle population that coexisted metastably with mixed micelles. With high Ch supersaturation, TCDC extracted L and Ch molecules from SUVs in different proportions to form Ch-supersaturated mixed micelles and Ch-enriched SUVs, in accordance with the metastable phase diagram. These experiments are consistent with the hypothesis that *sn*-1 palmitoyl L species are subselected for bile, in part, by physical-chemical interactions of intracellular BS concentrations with Ch-poor membranes and that the subsequent evolution of Ch-rich vesicles and Ch-saturated mixed micelles occurs via a transitional hexagonal (rod) phase. These liquid-crystalline states are likely to be transient in Ch-unsaturated biles, but may persist in Ch-supersaturated human biles because of their high Ch contents which retard or inhibit these phase transitions. —**Cohen, D. E., M. Angelico, and M. C. Carey.** Structural alterations in lecithin-cholesterol vesicles following interactions with monomeric and micellar bile salts: physical-chemical basis for subselection of biliary lecithin species and aggregative states of biliary lipids during bile formation. *J. Lipid Res.* 1990. **31:** 55-70.

Supplementary key words small unilamellar vesicles • multilamellar vesicles • mixed micelles • hexagonal phase rods • molecular species of lecithins • cholesterol • quasielastic light scattering • turbidimetry • gel filtration • phase analysis

During bile formation, bile salts (BS) stimulate the hepatocellular secretion of lecithin (L) and cholesterol (Ch) from hepatocytes. Concomitantly, bile becomes enriched with predominantly *sn*-1 palmitoyl L molecular species (1, 2). The relatively hydrophilic (or less hydrophobic) character of biliary L species, compared to other phospho-, glyco-, and sphingolipids of mammalian hepatocytes (1, 2), suggests that physical-chemical mechanisms may play a role in their "selection" for bile.

In the aqueous environment of the hepato-biliary tree, biliary lipid secretion and aggregation must be controlled, as a first approximation, by the phase equilibria of these lipid systems in water (3-5). For example, studies of model biles at both metastable and true equilibria (4, 5) have successfully predicted the presence in human biles of

Abbreviations: BS, bile salt(s); L, lecithin; Ch, cholesterol; TCDC, taurochenodeoxycholate; QLS, quasielastic light scattering; HPLC, high performance liquid chromatography; MLV, multilamellar vesicles; SUV, small unilamellar vesicles; CMC, critical micellar concentration.

[1]Present address: Clinica Medica III, II Cattedra di Gastroenterologia, Universita degli Studi di Roma "La Sapienza", Viale dell'Universita 37, 00185 Rome, Italy.

[2]To whom correspondence should be addressed at: Department of Medicine, Brigham and Women's Hospital. 75 Francis Street, Boston, MA 02115.

BS-L-Ch mixed micelles and L-Ch vesicles (6). Since biliary lipids are inaccessible to experimental sampling within hepatocytes, within canaliculi, and within the intrahepatic biliary tree, it is not known whether their equilibrium phase relations offer insights into biliary lipid aggregation during the metastable states of secretion, concentration, and transport throughout the biliary tree. On the basis of observations in model systems (3–5), it is unlikely that biliary lipids achieve equilibrium physical states during the rapid (15 to 45 sec) physiological transit times from cell to hepatic canaliculi and to the extrahepatic sites of bile sampling (7).

To obtain in vitro insights into these events, we characterized, kinetically and at equilibrium, interactions of the common primary BS, sodium taurochenodeoxycholate (TCDC), with model membrane vesicles under physical-chemical conditions likely to be encountered pathophysiologically. On the basis of time-dependent turbidimetry, we show that rates of BS dissolution from membranes composed of synthetic L molecular species with low Ch/L ratios accurately predict steady-state biliary L compositions. By using quasilastic light scattering (QLS), gel filtration, and phase analysis, we marshall evidence to suggest that, as bile is concentrated within the biliary tree, submicellar and micellar BS concentrations interact with unilamellar vesicles of L and Ch, resulting in a step-wise series of phase transformations leading from homogeneous vesicles to mixed micelles, possibly via an intervening hexagonal (rod-like) phase. Our studies also provide a phase equilibrium and kinetic explanation as to why BS can transform Ch-poor vesicles into Ch-rich vesicles that contain a Ch-to-L ratio as high as 2:1. Because Ch, in physiological concentrations, dramatically retards all of these transformations, we predict that each of these transitional phases could be pathophysiological constituents of freshly sampled extrahepatic biles.

EXPERIMENTAL PROCEDURES

A. Materials

Sodium salts of TCDC (Calbiochem, San Diego, CA) and of [U-^{14}C]taurine-labeled TCDC (prepared in this laboratory, 8) produced single spots (purity ~99%) after application of 200 μg onto thin-layer chromatography plates (4); radiolabeled TCDC was radiochemically pure upon zonal scanning. Grade I egg L (Lipid Products, South Nutfield, Surrey, U. K.) was of similar purity as judged by thin-layer chromatography (200 μg sample application, developing solvent $CHCl_3$-MeOH-H_2O 95:35:4, v:v:v). Ch (Nu-Chek-Prep, Elysian, MN) was recrystallized thrice from hot ethanol to achieve 99% purity by gas-liquid chromatography. Synthetic molecular species of L [*sn*-1 palmitoyl, *sn*-2 oleoyl (16:0–18:1); *sn*-1 palmitoyl, *sn*-2 linoleoyl (16:0–18:2); *sn*-1 palmitoyl, *sn*-2 arachidonoyl (16:0–20:4); *sn*-1 stearoyl, *sn*-2 oleoyl (18:0–18:1); *sn*-1 stearoyl, *sn*-2 linoleoyl (18:0–18:2); and *sn*-1 stearoyl, *sn*-2 arachidonyl (18:0–20:4)] were purchased from Avanti Polar Lipids, Inc. (Birmingham, AL). Approximately 200 μg of each L species gave a single spot by thin-layer chromatography and was more than 98% pure by both high performance liquid chromatography (HPLC) (1) and gas-liquid chromatography of their fatty acid methyl esters (1). The supplier ascertained by specific phospholipase hydrolysis that each L molecular species contained less than 20% fatty acyl chain racemization. Radiolabeled 1-palmitoyl-2-[1-^{14}C]oleoyl-*sn*-glycerophosphocholine (sp act 52.6 mCi/mmol) and [4-^{14}C]Ch (sp act 57.5 mCi/mmol) were of similar chemical and radiochemical purities (New England Nuclear, Boston, MA). Tris-HCl (hydroxymethyl-aminoethane hydrochloride) was obtained from Sigma (St. Louis, MO) and all other chemicals and solvents were ACS or reagent grade quality (Fischer Scientific Co., Medford, MA). Sepharose and Superose packing gels (see Methods) were purchased from Pharmacia (Piscataway, NJ). ACS grade sodium chloride was roasted at 600°C for 4 h in a muffle furnace to oxidize and remove organic impurities. Pyrex-brand glassware was acid-washed for 24 h (1 M HNO_3) followed by 24 h alkali-alcohol washing (EtOH–2 M KOH 1:1, v:v) and rinsed thoroughly with purified H_2O. All H_2O was filtered, ion-exchanged, and glass-distilled (Corning Glass Works, Corning, NY). To minimize oxidation of lipids during model membrane preparation and experimentation, freshly purified water was boiled for 10 min and cooled to room temperature under a stream of argon.

Methods

1. Multilameller vesicles (MLVs). After coprecipitation from stock solutions in chloroform–methanol 1:1 (by vol) (4), dried L films (with and without Ch) were resuspended in aqueous buffer (5 mM Tris-HCl, 0.15 M NacL, pH 7.4) that included 3.0 mM of NaN_3 as microbial inhibitor to give concentrations of 0.5 mM L and 0–0.17 mM Ch. Unless otherwise specified, this buffer was used in all subsequent studies. Aqueous lipid dispersions were sealed under nitrogen, and sufficient energy to form MLVs (9) was provided by a water-bath sonicator (Laboratory Supply Inc., Hicksville, NY) set at 80 watts for 15 min at room temperature (~23°C). As detailed below, MLVs prepared in this manner yielded reproducible turbidities. Following sonication, MLVs were equilibrated at 37°C for a further 2–3 h prior to experimentation.

2. Small unilamellar vesicles (SUVs). Dried L and Ch lipid films, prepared as above, were resuspended in filtered (polycarbonate 0.4 μm filters, Bio-Rad Labs, Richmond, CA) buffer to give final concentrations of 10.0 mM L and 0–10.0 mM Ch. SUVs were prepared by sonication using

a titanium probe fitted to a Branson W 185 sonifier (Heat Systems Inc., Plainview, NY) set at 50 watts. Times required to complete the sonication process varied from 30 min for SUVs of pure L to 120 min at the highest Ch contents (10 mM). To minimize heat-induced degradation of L (10), sonication was performed at 4°C under an argon atmosphere. Because prolonged sonication ($\geq$1 h) also results in substantial oxidation of polyunsaturated fatty acyl chains of L molecules (11), egg yolk L (which contains a variety of polyunsaturated fatty acyl chains) was excluded from SUVs requiring > 30 min sonication periods (i.e., those containing Ch). Sonicated samples were ultracentrifuged (SW 50.1 rotor) in a model L5-65 ultracentrifuge (Beckman Instrument Co., Fullerton, CA) at 100,000 *g* for 1 h (4°C) to remove titanium fragments (10) and MLV assemblies (12). SUVs prepared in this fashion yielded reproducible distributions of sizes as assessed by QLS and gel filtration (see below). To minimize variations in the distribution of SUV sizes due to spontaneous SUV aggregation (13, 14), experiments were performed within 24 h of SUV preparation. Supernatants containing SUV fractions were diluted with the same buffer to give final lipid concentrations of 2.5 mM L and 0–2.5 mM Ch as determined by chemical analysis (see below).

3. Turbidimetry. Transmission spectrophotometry was used in measuring BS dissolution rates of MLVs. Absorbances at 600 nm were monitored as functions of time using a Cary 118C double-beam UV-VIS spectrophotometer (Varian, Palo Alto, CA) essentially as described by Lichtenberg et al. (15). Disposable cuvettes with 1 cm lightpaths (Fisher Scientific, Medford, MA) were temperature-controlled to 37°C using a calibrated Lauda model K-2/RD Flow Thermostat heat exchanger (Lauda, Königshafen, West Germany).

4. Quasielastic light scattering (QLS). QLS measurements of TCDC-SUV interactions were performed on a home-built apparatus. Configuration of the apparatus and computer has been described in detail elsewhere (16). In brief, we used a Spectra Physics (Mountain View, CA) model 164 argon ion laser tuned to 5145 Å and a home-built thermostatted sample holder based on the Peltier principle. All light-scattering measurements were performed at a scattering angle of 90°C and a sample temperature of 37°C. The intensity autocorrelation function of scattered light was collected using a 64-channel Langley-Ford (Amherst, MA) model 1096 correlator, to which a Digital (Maynard, MA) Pro 350 model computer was interfaced. The autocorrelation function was analyzed primarily by the method of cumulants (17) which yielded the mean diffusion coefficient ($\overline{D}$) of particles in solutions and percent variance (V), a polydispersity index. The correlator was equipped with an algorithm for rapid (<5 sec) cumulants analysis which permitted autocorrelation functions accumulated during 20–30 sec intervals to be analyzed immediately. This allowed us to characterize kinetic interactions of TCDC and SUVs by repeated measurements of $\overline{D}$ and V (see below). In certain cases where V values exceeded 60%, intensity autocorrelation functions were further analyzed for one, two, or three coexisting particle populations by multi-exponential analysis as described elsewhere (16). In these cases, two-component analysis provided the best computer fits and the $\overline{D}$ value of each particle population as well as their relative concentrations (w/w) were obtained. The $\overline{D}$ value of each particle population was then translated into the mean hydrodynamic radius ($\overline{R}_h$) by the Stokes-Einstein relationship utilizing the viscosity of the solvent (5).

5. Gel filtration. Lipid aggregates formed by equilibrated TCDC and SUV mixtures were isolated employing gel filtration at 12–24 h and, in some cases, at later time points. Sepharose 4B gel (Pharmacia, Piscataway, NJ) was packed in a Pharmacia C10/40 column to give a gel bed length of 35 cm. Calibration of the columns was performed using uniform polystyrene spheres of 910 Å and 380 Å diameter (Seragen Diagnostics, Indianapolis, IN). To prevent aggregation of the spheres, ~1% (w/v) Triton X-100 (Baker, Phillipsburg, NJ) was added to the eluting buffer. We achieved removal of nonionic detergent by washing the column with 10 volumes of the same buffer. A prepacked and calibrated Pharmacia HR10/30 Superose 6 column was used in some experiments.

6. Ultracentrifugation. To determine aqueous monomeric concentrations of TCDC, we first equilibrated pre-formed SUVs for 24 h with several TCDC concentrations at 37°C. These mixtures were then ultracentrifuged in a TLA100.2 rotor for 22 h at 380,000 *g* using a model TL-100 ultracentrifuge (Beckman Instruments, Fullerton, CA). After braking of the ultracentrifuge, the tubes were removed gently so as not to disturb the separated phases. In order to dissipate possible TCDC monomer gradients by self-diffusion, the systems were allowed to re-equilibrate at 37°C for 1 h (18).

C. Experimental design

1. BS dissolution of MLVs. We first established stable baseline absorbances of each MLV preparation prepared from the synthetic Ls (A_{600} = 0.75 ± 0.05). We then transferred 2.0 ml of each MLV preparation to prewarmed cuvettes (37°C) containing the required mass of TCDC (dried from methanol) to give final TCDC concentrations of 5.0 mM. The cuvettes were gently mixed for 15 sec to allow complete dissolution of the dried TCDC. The samples were then transferred to the spectrophotometer, where absorbances at 600 nm were monitored as functions of time until stable values were obtained.

2. BS Interactions with SUVs. a. Time-dependence. We first established, using QLS, baseline $\overline{R}_h$ and V values of

240-μl samples of SUVs at 37°C. This was followed by layering 60 μl of a BS solution (0.5–40 mM) in buffer onto the top of the SUV suspension using a prewarmed microsyringe (Hamilton, Reno, NV). Such mixtures were designed to give a final L concentration of 2.0 mM and TCDC concentrations that varied from 0.1 to 8.0 mM. The QLS tubes were then vortex-mixed for approximately 2 sec, replaced in the sample holder, and $\overline{R}_h$ and V values were monitored as functions of time until both values stabilized. We found that QLS data collections begun within 10–15 sec after vortex mixing yielded spurious $\overline{R}_h$ and V values that were not reproducible, possibly due to transient currents or small air bubbles induced by the mixing process. Therefore, all QLS data were collected at least 15 sec after mixing. To standardize measurements of $\overline{R}_h$ and V, which varied as functions of time, sample time settings (i.e., channel width) of the correlator required frequent updating. Each new sample time was chosen so that the total decay time for the intensity autocorrelation function (i.e., 64 channels × sample time per channel) was approximately twice the decay time actually required (16). Therefore, since all other variables (scattering angle, temperature, ionic strength, etc.) were held constant, time-dependent changes in $\overline{R}_h$ and V values of samples with different lipid compositions could be compared directly. In the absence of added TCDC, no change was detected in the $\overline{R}_h$ or V values of SUVs for up to 72 h, indicating that, over the time period of experiments reported, all SUV preparations were stable.

b. Particle size analysis at equilibrium. Dispersions of SUVs were fractionated by gel filtration prior to and 12–24 h after addition of TCDC solutions. Because Sepharose 4B particles can bind SUVs during gel filtration, columns were presaturated with an identical SUV suspension in buffer to exclude such artifacts. To preserve mixed micellar integrity in systems that resulted in the formation of mixed micelles, columns were pre-equilibrated with buffer containing 2.0 mM TCDC, the CMC of TCDC (18). Because, in preliminary experiments, micellar TCDC concentrations were found to displace SUVs from Sepharose 4B binding sites, columns pre-equilibrated with TCDC were not simultaneously saturated with SUVs.

c. Inter-vesicular BS concentrations. Solutions of [^{14}C]TCDC were added to each SUV suspension (as in section 2a, above) to give final TCDC concentrations ranging from 0.4 to 2.0 mM and were allowed to equilibrate for 12–24 h. After pelleting of the SUVs by ultracentrifugation, the samples were re-equilibrated for 1 h at 37°C. This time was chosen on the basis of bulk-to-surface equilibration times of adsorbed TCDC films in concentrations below the CMC (18), with the result that any TCDC monomer gradient that may have developed during ultracentrifugation was dissipated. After monomer equilibration, no QLS autocorrelation function developed in the supernatants, demonstrating that they were free of vesicles and micelles. We then quantified monomeric TCDC concentrations in the supernatants by scintillation counting (see below).

D. Analytical procedures.

Concentrations of L were determined by the choline oxidase method (19) or by the inorganic phosphorus procedure (4). We determined TCDC concentrations enzymatically using 3α-hydroxysteroid dehydrogenase (4) and measured Ch concentrations by gas–liquid chromatography (Shimadzu model GC9a, Kyoto, Japan) (20). We assayed lipids radiolabeled with ^{14}C by liquid scintillation counting using a Beckman (Fullerton, CA) model LS-7500 scintillation counter and a hydrofluor scintillant (National Diagnostics, Highland Park, NJ).

RESULTS

BS dissolution of MLV

Fig. 1 displays the turbidities of MLVs plotted as percent "initial"[3] absorbance as functions of time after mixing with dry TCDC. For each of the *sn*-1 16:0 L species with differing carbon number and degrees of unsaturation of the *sn*-2 fatty acyl chain, absorbances declined rapidly over ~8 min. Addition of a second double bond to the *sn*-2 C-18 chain slightly retarded dissolution, whereas lengthening of the *sn*-1 fatty acyl chain markedly decreased the dissolution rates.

Fig. 2 plots, in the same format, the influence of *sn*-1 fatty acyl chain length on dissolution rates of two identical *sn*-2 18:1 L species, as well as the effects of increasing the Ch/L molar ratio of the MLVs from 0 to 0.3. Micellar (5 mM) TCDC dissolution of 16:0–18:1 L (Fig. 2A) was appreciably faster than that of 18:0–18:1 L (Fig. 2B) for equivalent Ch/L molar ratios.[4] These results show that Ch

[3]Rajagopalan and Lindenbaum (21) showed by turbidimetry that, during BS dissolution of MLV, two components were distinguishable in the absorbance decay. An initial rapid fall in absorbance to ~30–60% of baseline took place over the first 30 sec, and this was followed by a slow decrease in turbidity over the next 10 min to several hours. Following these authors, the first section of the dissolution curve was kinetically complex and was excluded from our analysis. In accordance with reference 21, MLV dissolution kinetics were compared by considering the absorbance at 1 min to be the "initial" turbidity.

[4]Turbidity is proportional to MLV size and concentration. To ensure that differences in MLV dissolution rates were due to L species and not to artefacts in MLV size and surface geometries, we compared the TCDC dissolution kinetics of MLV composed of 16:0–18:1, egg yolk, and 18:0–18:1 L by turbidimetry with the TCDC dissolution kinetics of SUVs composed of the same L species and all of similar diameter by light scattering. In each case, the concentration TCDC was 5.0 mM and the SUV concentration was 1.5 mM. By monitoring percent initial scattered laser light intensity (i.e., intensity prior to mixing) as functions of time, it was apparent that the rank order for TCDC dissolution of MLVs composed of the three L species was identical to that for TCDC dissolution of the SUVs. It is unlikely, therefore, that different TCDC dissolution rates in experiments employing MLVs are due to variations in surface geometries and aggregate sizes.

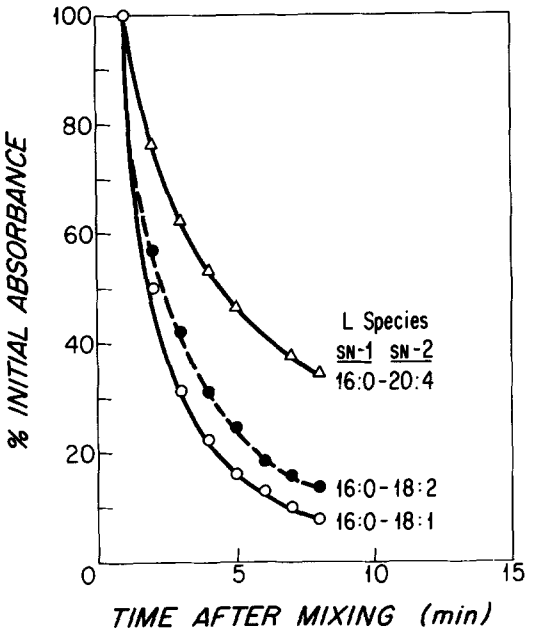

Fig. 1. Bile salt dissolution of multilamellar vesicles (MLVs) measured by turbidimetry at 600 nm: Percent of initial absorbance[3] is plotted as functions of time in min following mixing TCDC (final concentration, 5.0 mM) with MLVs composed of 0.5 mM of synthetic *sn*-1 16:0 lecithins (L) with the principal unsaturated fatty acids of biliary L in the *sn*-2 position: 18:1 (oleic), 18:2 (linoleic), and 20:4 (arachidonic). Other conditions were 5.0 mM Tris- HCl, 0.15 M NaCl, 3.0 mM NaN_3, 37°C, pH 7.4

retards TCDC dissolution of both L species in proportion to increases in its MLV concentration.

Fig. 3 plots the half-times ($T_{1/2}$) for 5 mM TCDC dissolution of MLVs as functions of all L molecular species studied as well as their as their Ch/L molar ratios. In the absence of Ch (point 0), TCDC dissolution rates were faster for all *sn*-1 16:0 L compared with *sn*-1 18:0 L species; however, 16:0-20:4 L species was an exception. In general, increases in Ch/L molar ratio increased $T_{1/2}$ (slowed dissolution rates) with a magnitude and pattern that varied markedly with each L molecular species. In cases of 16:0-18:1, 16:0-18:2, and 18:0-20:4 L, Ch induced curvilinear and nearly parallel increases in $T_{1/2}$ values with a weaker effect at Ch/L ratios of 0.05-0.1, compared with Ch/L ratios of 0.2 and 0.3. The three other L species did not follow this pattern; in the case of 18:0-18:1 L, progressive increases in Ch content dramatically slowed the dissolution rates at all Ch/L molar ratios. In the case of 18:0-18:2 L, no dissolution-retarding influence of Ch was noted until the Ch/L ratio reached 0.3. In contrast, the dependencies of $T_{1/2}$ values of 16:0-20:4 L on Ch/L ratio were sigmoidal, with the value for the highest Ch/L ratio being no different from that at a Ch/L ratio of 0.2.

BS interactions with SUVs

Fig. 4 displays, in composite format, the time-dependence of $\bar{R}$ and V values of SUVs as the TCDC concentration was increased from below to above the CMC value (2.0 mM).[5] Each panel shows the result for three L species: two synthetic L species (16:0-18:1, 18:0-18:1), and natural egg yolk L, which contains a high proportion of these L species (1). Fig. 4A shows the influence of 0.4 mM TCDC (<CMC) on the $\bar{R}_h$ and V values of the SUVs as functions of time after mixing. As depicted in the upper panel, there was a small initial increase in $\bar{R}_h$ values from 330 Å to 370 Å and 260 Å to 280 Å at 0.5 min for SUVs composed of egg yolk and 16:0-18:1 L, respectively, without a change for the more hydrophobic 18:0-18:1 L.

[5]In preliminary experiments, the concentration of L in SUVs (2.0 mM after addition of TCDC) was chosen so that the scattered light intensity was sufficient to provide reproducible mean hydrodynamic radii (± 5-10%) for QLS measurements within 20-30 sec. In all experiments, the most rapid and dramatic changes occurred as particles increased in size (Figs. 4 and 6) with a concomitant increase in scattered light intensity, helping to minimize errors associated with the relatively short data collection periods. At the highest added TCDC concentration (Figs. 4D and 6C), particle sizes decreased to those characteristic of micelles at a slower rate than the initial size increase. This allowed us to use longer data collection times in order to compensate for the decreased intensity of scattered light.

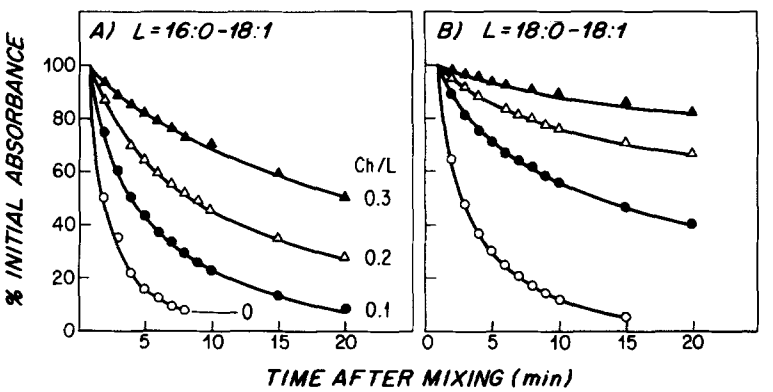

Fig. 2. Bile salt dissolution of MLVs of two L molecular species containing Ch/L molar ratios of 0-0.3 measurement by transmission spectrophotometry at 600 nm. Percent of initial absorbance[3] is plotted as functions of time following mixing TCDC (final concentration, 5.0 mM) with MLVs composed of 0.5 mM 16:0-18:1 L (A) and 18:0-18:1 L (B). In each panel, increases in Ch/L molar ratios are displayed by different symbols (Ch/L ratios labelled in panel A). Other conditions were 5.0 mM Tris HCl, 0.15 M NaCl, 3.0 mM NaN_3, 37°C, pH 7.4.

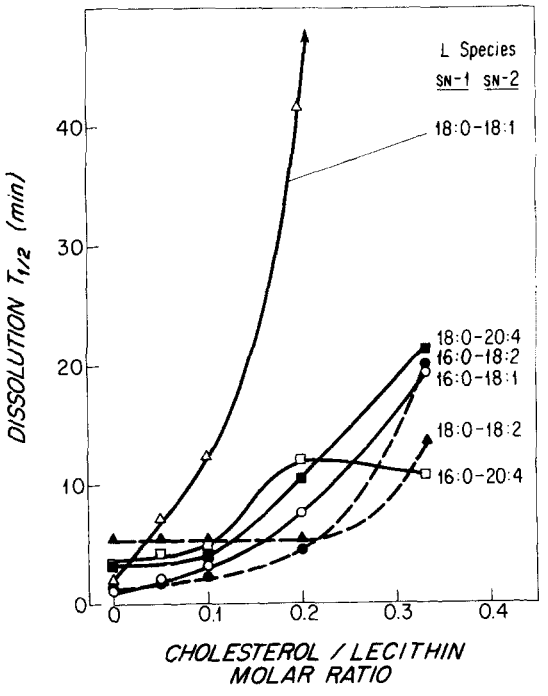

Fig. 3. Half times ($T_{1/2}$) in min for TCDC dissolution of MLVs, plotted as functions of Ch/L molar ratio for the principal L molecular species of human bile, as shown by the inscribed labeling. The anomalous behavior of 16:0-20:4 L at the highest Ch/L molar ratio is described in the text. Other conditions were 0.5 mM L, 5.0 mM TCDC, 5.0 mM Tris-HCl, 0.15 M NaCl, 3.0 mM NaN_3, 37°C, pH 7.4.

The initial increase in SUV sizes was followed by a decline to original values over 1.0 to 2.5 min. As displayed in the lower panel (Fig. 4A), V values ranged from 30 to 40% and showed no systematic changes over time. Fig. 4B demonstrates the time-dependent influences of 1.0 mM TCDC (<CMC) on both $\overline{R}_h$ and V values of the SUVs. As shown in the upper panel, this concentration of TCDC produced a sharp decrease in $\overline{R}_h$ values over the first 2.0 min, being most pronounced with egg yolk L (320→270 Å). As shown in the lower panel, parallel decreases in V values occurred taking approximately 6 min to stabilize. Fig. 4C demonstrates the influence of 2.0 mM TCDC (approximately the CMC) on $\overline{R}_h$ and V values of SUVs as functions of time following mixing. As displayed in the upper panel, after an initial lag time of 2 to 10 min, dramatic sigmoidal increases in $\overline{R}_h$ values occurred, stabilizing at approximately double the initial sizes at 10-30 min. This occurred very quickly for egg yolk L and slowly for *sn*-1 18:0 L, with intermediate rates for 16:0-18:1 L. Concomitantly, all V values (lower panel), which were approximately 40% initially, decreased curvilinearly over 5-10 min and stabilized at very low values of 2-5%. The V values changed fastest for SUVs composed of 16:0-18:1 and egg yolk L and slowest for the 18:0-18:1 L species. Fig. 4D displays the QLS results for the time-dependent interactions of 4.0 mM (i.e., micellar) TCDC with SUVs of the three L species. Immediately after mixing, there were striking rapid increases in $\overline{R}_h$ values to reach sizes that were somewhat less than those achieved at approximately the CMC of TCDC (Fig. 4C, upper panel). After brief (<2 min) plateaus in $\overline{R}_h$ values, a curvilinear decline in sizes occurred, reacing final $\overline{R}_h$ values of 60-75 Å within 5 to 10 min in the rank order: 16:0-18:1 L > egg yolk L > 18:0-18:1 L. During the time interval that the $\overline{R}_h$ values increased abruptly, peaked, and slowly declined, V values (lower panel) fell to a nadir-value at the $\overline{R}_h$ peak, then increased reciprocally in curvilinear fashion, mirroring the fall in $\overline{R}_h$ values, and declined again as the $\overline{R}_h$ values reached their smallest sizes.

Not displayed here are the results for the interactions of 0.4 mM-4.0 mM TCDC with SUV, when the SUVs con-

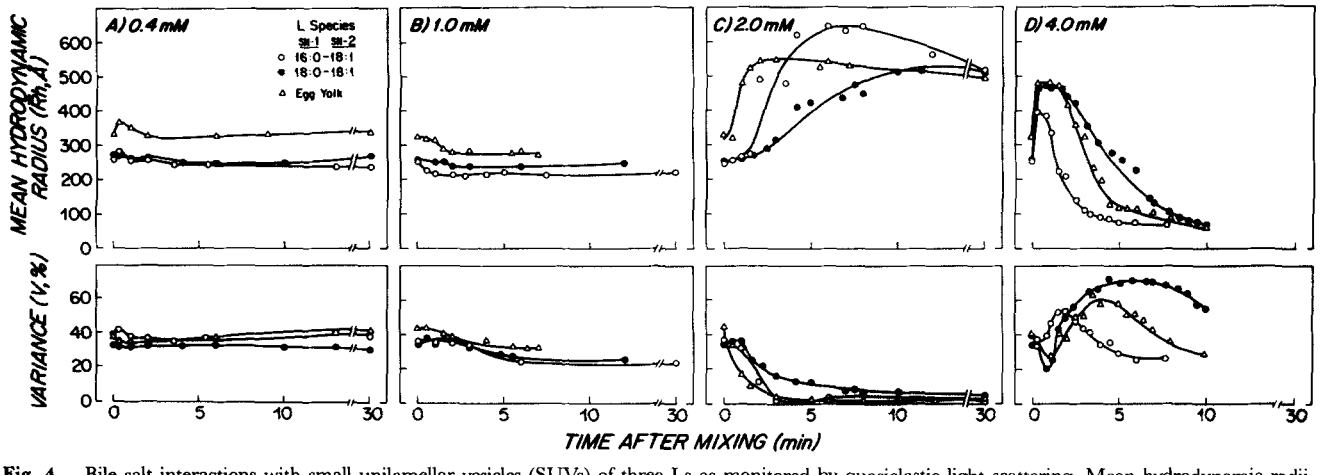

Fig. 4. Bile salt interactions with small unilamellar vesicles (SUVs) of three Ls as monitored by quasielastic light scattering. Mean hydrodynamic radii, $\overline{R}_h$, in Å (top panel), and variances, V, (bottom panel) are plotted as functions of time following mixing. Two mM SUVs were composed of 16:0-18:1 (○), 18:0-18:1 (●), and egg yolk L (△). TCDC was added to give final concentrations that ranged from well below to well above its critical micellar concentration of 2.0 mM under the conditions of the experiments: (A) 0.4 mM, (B) 1.0 mM, (C) 2.0 mM and (D) 4.0 mM TCDC. Other experimental conditions were 0.15 M NaCl, 5.0 mM Tris HCl, 3.0 mM NaN_3, 37°C, pH 7.4.

tained systematic increases in Ch content (Ch/L = 0.33–1.00). All of the changes in $\overline{R}_h$ and V values noted in Fig. 4 occurred with systematic increases in TCDC concentration, but the rates were progressively retarded in proportion to the Ch content. Further, the marked differences due to L molecular species noted in Fig. 4 were obliterated with increases in the Ch content of the SUVs.

Fig. 5 (A–D) demonstrates the egg yolk L elution profiles by Sepharose 4B gel filtration analysis (see Methods) of equilibrated systems for which the kinetic data by QLS analysis were presented in Fig. 4 (A–D) Fig. 5A depicts the L elution profile of SUVs composed of egg yolk L after equilibration with 0.4 mM TCDC. By comparison with calibration standards (see Methods), the major peak of SUVs eluted halfway between V_o and V_t at the Stokes' radius of 100 Å with a small base-line separated peak at the void volume with a $\overline{R}_h$ value of 500 Å as determined by QLS. Compared with the elution profile of pure (no TCDC) SUVs (data not shown), this profile showed no appreciable change in SUV sizes or their distribution. Because the small population of larger SUVs (Fig. 5A) contributed significantly to the scattered light intensity (16), the overall $\overline{R}_h$ value was 330 Å, as displayed by the time zero value for egg yolk L SUVs in Fig. 4A. Ultracentrifugal phase separation and monomeric BS analysis of this system at equilibrium revealed that 0.33 mM TCDC (83%) was bound to egg yolk L SUVs. Therefore, we carried out pre-equilibration of the column with the unbound TCDC concentration (0.07 mM) and eluted the vesicles with the same TCDC concentration. These results revealed that the elution profile using 0.07 mM TCDC was identical to that shown in Fig. 5A (data not shown).

Fig. 5B displays the elution profile by gel filtration of egg yolk L SUVs after the addition of 1.0 mM TCDC (same system as in Fig. 4B). The profile shows a single homogeneous population of SUVs with a mean Stokes' radius of 275 Å as derived from Sepharose 4B calibration standards. Because there is a single population of vesicles in this elution profile (Fig. 5B), i.e., no other L peaks or shoulders, the Stokes' radius is identical to the $\overline{R}_h$ value obtained by QLS for egg yolk L SUVs after 2 min of mixing with 1 mM TCDC (Fig. 4B). After equilibration, ultracentrifugation of this system indicated that 0.7 mM TCDC (70%) was bound to the egg yolk SUVs. Column pre-equilibration and elution with the unbound TCDC concentration (0.30 mM), as determined by ultracentrifugation, had no influence on the results displayed in Fig. 5B (data not shown).

Fig. 5C shows the elution profiles by gel filtration of egg yolk L SUVs after equilibration with 2.0 mM TCDC (~CMC). Two dissimilar particle populations are clearly evident: larger aggregates eluting at the position of V_o with $\overline{R}_h$ values of 500 Å (by QLS), and smaller L aggregates with Stokes' radius of 100 Å eluting in the included volume. After ultracentrifugation and analysis, most of the TCDC (1.63 mM, 82%) was bound to the L particles at equilibrium. After column pre-equilibration and elution with the free monomeric concentration of 0.37 mM TCDC, equilibrated systems were not appreciably different from the gel filtration results displayed in Fig. 5C. Be-

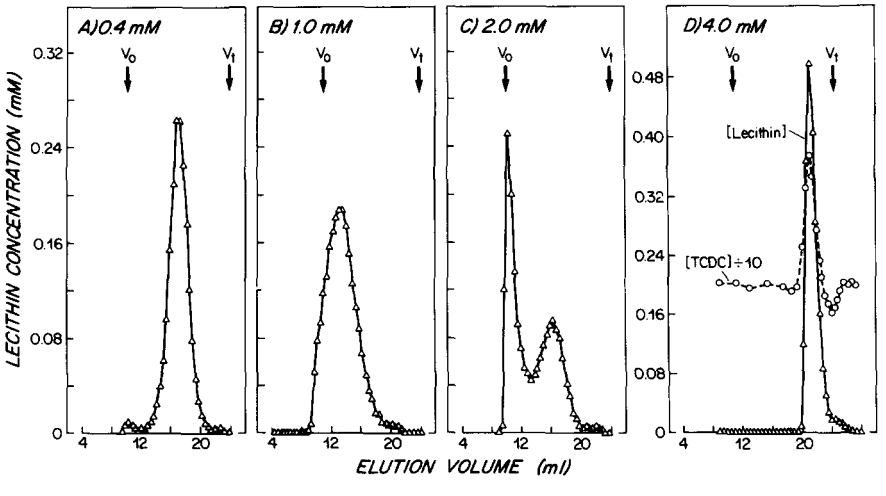

Fig. 5. Sepharose 4B gel permeation chromatography of 24 h equilibrated TCDC-SUV mixtures identical to those studied kinetically in Fig. 4. Lecithin concentrations are plotted as functions of elution volume (ml) for SUVs composed of 2.0 mM egg yolk L following 24 h equilibration with TCDC in concentrations of (A) 0.4 mM, (B) 1.0 mM (C) 2.0 mM, and (D) 4.0 mM. Buffer conditions were 0.15 M NaCl, 5.0 mM Tris HCl, 3.0 mM NaN_3 at pH 7.4 (20°C). For mixture D, which contained 4.0 mM TCDC, the column was pre-equilibrated and eluted with buffer containing 2.0 mM TCDC (approx. CMC) to preserve micellar integrity. In cases A-C, no changes in elution profiles occurred when columns were pre-equilibrated and eluted with the measured intervesicular monomeric TCDC concentration or at 48 and 96 h (see text). Void volume (V_o) and total volume (V_t) are indicated by arrows. Sizes of lipid particles (mean hydrodynamic and Stokes radii) were derived by QLS and calibration standards.

cause of the slight possibility that 24-h equilibration times might be insufficient to detect changes in the proportions of the large and small particles in Fig. 5C, we repeated the gel filtration experiments without 0.37 mM TCDC at 48 and 96 h and found no differences, compared with the results at 24 h (Fig. 5C).

Fig. 5D shows the gel filtration elution profiles of egg yolk L SUVs after equilibration with 4 mM (micellar) TCDC. Because the final particle sizes by QLS (Fig. 4D) suggested that the equilibrated systems with this TCDC concentration were composed of large mixed micelles, the Sepharose 4B column was pre-equilibrated and eluted with 2.0 mM TCDC (~CMC of TCDC, 18). All L plus TCDC molecules in excess of the CMC coeluted as particles of approximately 45 Å in Stokes' radius, in satisfactory agreement with the QLS sizes for egg yolk L-TCDC micelles (60 Å) in Fig. 4D.

Fig. 6A displays the $\bar{R}_h$ values of mixtures of two SUV populations composed of the synthetic Ls (16:0-18:1 and 18:0-18:1) and Ch in a Ch/L molar ratio of 0.33 as functions of time after mixing with 8.0 mM (>CMC) TCDC. In both cases, there was an initial rapid rise in $\bar{R}_h$ values to reach a peak at 0.5 and 2 min, respectively, followed by a slow decrease to $\bar{R}_h$ values of approximately 50 Å. Over the next several hundred minutes, the $\bar{R}_h$ values increased again to give intermediate values. In both cases, interactions of TCDC with 16:0-18:1 L SUVs occurred more rapidly; timed variations in V values (data not shown) paralleled those observed for SUVs containing no Ch in the presence of supramicellar TCDC (see Fig. 4D). At $\bar{R}_h$ values of 50 Å (trough in Fig. 6A), V values were less than 50% but, at apparent equilibrium (300-2000 min), they were greater than 50- 60%. These results suggested that two or more discrete particle populations coexisted at the termination of these experiments. We tested this hypothesis by a multiexponential method (16). At apparent equilibrium (2000 min, Fig. 6A), the intensity autocorrelation function was best modelled as two components, suggesting that two particle populations coexisted in each system. The $\bar{R}_h$ values of the smaller sized particles, that comprised 98.2% to 99.8% of total solute masses, were 36 Å for 16:0-18:1 L and 32 Å for 18:0-18:1 L, consistent with the sizes of mixed micelles (5). The $\bar{R}_h$ values of the larger sized populations, 380 Å for 16:0-18:1 L and 410 Å for 18:0-18:1 L, were consistent with vesicles. We attempted to isolate the larger aggregates using an eluent concentration of 2 mM TCDC and Superose 6 gel filtration chromatography but, because of the low solute masses (1.8%, 0.2% of total lipids, respectively), the quantities isolated were insufficient to permit measurement of their relative lipid compositions.

Figs. 6B and 6C plot the time-dependent $\bar{R}_h$ values following mixing 8.0 mM (>CMC) TCDC with SUVs

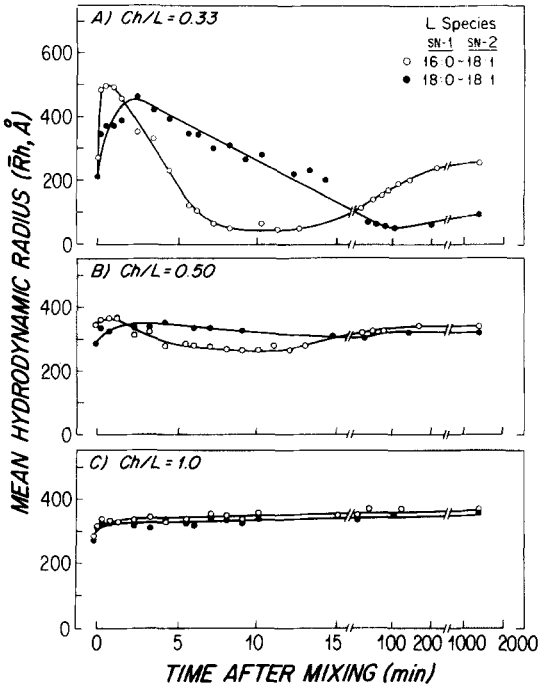

Fig. 6. Bile salt interactions with Ch/L SUVs as functions of increases in Ch/L ratio and time. Mean hydrodynamic radii, $\bar{R}_h$, in Å, are plotted as functions of time after mixing TCDC (final concentration 8.0 mM) with a 2.0 mM concentration of SUVs composed of two synthetic L molecular species. Ch/L ratios were (A) 0.33, (B) 0.50, and (C) 1.0. Other conditions were 0.15 M NaCl, 5.0 mM Tris HCl, 3.0 mM NaN_3, 37°C, pH 7.4.

containing Ch/L in molar ratios of 0.5 and 1.0, respectively. As will be shown below, both relative lipid compositions were well outside the mixed micellar zone for the total lipid compositions. With SUVs containing a Ch/L molar ratio of 0.5 (Fig. 6B), the time-dependent $\bar{R}_h$ values were slightly reminiscent of those SUVs with Ch/L = 0.33 (Fig. 6A). Small initial increases in $\bar{R}_h$ values were followed by modest decreases and then final increases, all falling in the 250-350 Å range. With SUVs containing a molar Ch/L ratio of 1.0 (Fig. 6C), 8 mM TCDC induced initial increases in $\bar{R}_h$ values which were followed by slight upslopes that continued for approximately 1500 min. The slight differences noted between the two L species at a Ch/L ratio of 0.5 (Fig. 6B) were abolished when the Ch/L ratio was increased to 1.0 (Fig. 6C).

Fig. 7 plots Superose 6 gel elution profiles of Ch/16:0-18:1 L SUVs (Ch/L molar ratio = 1.0) before Fig. 7A) and after (Fig. 7B) equilibration with 8.0 mM TCDC. Prior to addition of TCDC, the SUVs eluted principally at the void volume ($\bar{R}_h$ values of 275 Å) with a smaller shoulder on this peak; no other particles were detected in the included volume. After equilibration with

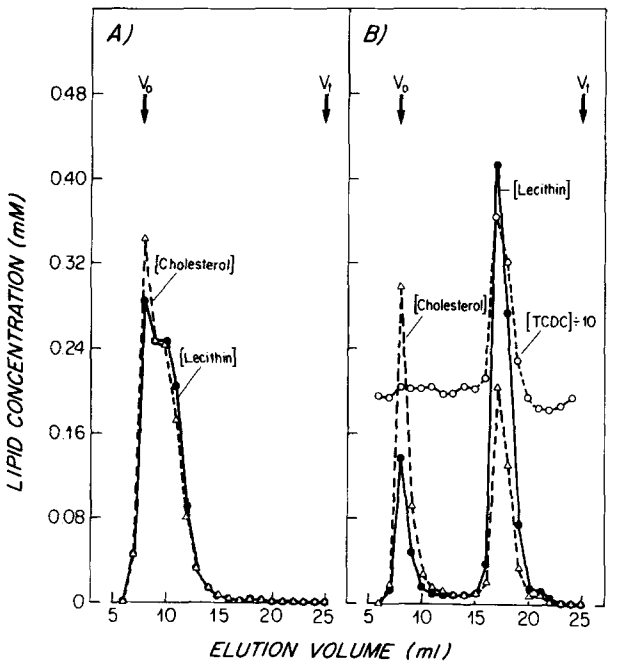

Fig. 7. Superose 6 gel permeation chromatography of SUVs composed of 2.0 mM 16:0-18:1 L and Ch in a Ch/L ratio of 1.0 (A) before and (B) following 24 h equilibration with 8.0 mM TCDC. Lipid concentrations as indicated for L (●), Ch (△) and TCDC ÷ 10 (○) are plotted as functions of elution volume. Other conditions were 0.15 M NaCl, 5.0 mM Tris HCl, 3.0 mM NaN_3, pH 7.4, 20°C. In panel B, after equilibration with TCDC, 2.0 mM TCDC (the CMC) was added to the buffer to preserve mixed micellar integrity.

TCDC (Fig. 7B) two particle populations eluted when the CMC of TCDC (2 mM) was used to pre-equilibrate and elute the column. One population of particles ($\overline{R}_h$ value of 350 Å) eluted at the void volume, consistent with SUVs. Compared with a molar ratio of 1.0, prior to addition of TCDC (Fig. 7A), the Ch/L molar ratio of these SUVs was 1.9. A smaller population of particles of micellar size (30 Å Stoke's radius) contained all of the TCDC in excess of the eluting buffer concentration (2 mM). The Ch/L ratio in this peak was 0.6, typical of Ch-supersaturated mixed micelles (5).

DISCUSSION

The primary aim of this study was to probe, by complementary physical-chemical methods, the dynamic and equilibrium physical-chemical states of biliary lipids during simulated bile formation. To simulate physiological conditions, we approached this problem in vitro through interactions of synthetic L/Ch vesicles with increasing TCDC concentrations that increased from well below to well above the CMC. As a corollary, we serendipitously found that this information shed insights on physical-chemical interactions between BS and membrane L that could, in part, be responsible for biliary L subselection.

Biliary L subselection

Two experimental observations indicate that BS might directly mediate biliary L subselection. First, the rate of transhepatic BS flux as well as the hydrophilic-hydrophobic balance of BS species influence L (and Ch) secretion rates into bile (22). Second, bile is selectively enriched in the least hydrophobic molecular L species of hepatocytes, e.g., *sn*-1 palmitoyl (16:0), with *sn*-2 oleoyl (18:1), linoleoyl (18:2), and arachidonyl (20:4) fatty acids (1). These molecular species of L elute earliest on reversed-phase HPLC columns (i.e., are least hydrophobic), suggesting that their relative hydrophilic character may contribute to their subselection from other hepatocyte Ls for secretion into bile (1, 2). Although hepatocellular BS concentrations are well below their CMC values (23), it is likely that canalicular BS concentrations are within the peri-micellar range (24). Therefore, turbidimetric dissolution rates of MLVs using micellar TCDC, as well as qualitatively similar behavior with SUVs, allow for a quantitative analysis of BS-binding of different L molecular species in the presence of variations in Ch content.

The present studies demonstrated that BS dissolved L from MLVs composed of less hydrophobic L more quickly than L from those composed of more hydrophobic species (Figs. 2 and 3). Interaction rates of submicellar as well as micellar BS concentrations and SUVs composed of synthetic L species paralleled these trends. Further, SUVs composed of egg yolk L, a mixture that included 16:0-18:1 and 18:0-18:1 Ls, gave intermediate interaction and micellar dissolution rates (Fig. 4). The sole exceptions were MLVs composed of 16:0-20:4 L. Although this L species eluted early by HPLC (1, 2) and was, therefore, less hydrophobic than 16:0-18:2 L, TCDC dissolved MLVs of this L slowly. The anomalous physical-chemical behavior of 16:1-20:4 L has been noted previously. For example, Middelkoop et al. (25) reported that the erythrocyte membrane "flip-flop" rates of 16:0-20:4 L were considerably slower than those for 16:0-18:2 L.

On the basis of the slower exchange rates of *sn*-1 16:0 Ls compared with *sn*-1 18:0 Ls between high density lipoproteins and chylomicrons, it has been suggested that the *sn*-1 fatty acid is the principal anchoring moiety of Ls in membranes (26). This was borne out in the present study; the *sn*-1 18:0 L species were most resistant to the interaction or dissolution effects of BS than the *sn*-1 16:0 Ls. Although this effect is presumably due to the closer molecular packing of longer chain *sn*-1 Ls in membranes, another important factor could be the lower liquid-crystalline transition temperature of the fatty acyl chains. Nevertheless, our ex-

periments were performed at 37°C, which exceeded the order-disorder transition temperatures of all L species employed in this study (most <0°C) (27) and, thereby, could not contribute to the different TCDC-vesicle interactions between L molecular species.

As noted in Results (Fig. 3), the influence of Ch on BS-MLV as well as BS-SUV interactions was concentration-specific for several L species. Of particular interest is the anomalous behavior of 16:0-20:4 L in the presence of Ch, with a slightly retarded dissolution rate between a Ch/L ratio of 0.1 and 0.2 and no further changes at the highest Ch concentration (Ch/L = 0.33). The increased Ch-induced resistance of other L bilayers to BS dissolution (Fig. 3) is in good agreement with the known condensing effect of the sterol on Ls with unsaturated acyl chains (28). On this basis, the 16:0-20:4 L species was the least condensed at the highest Ch/L ratio; this effect may be of pathophysiological importance, as discussed below.

Recent evidence suggests that BS promote the formation of pericanalicular vesicles within hepatocytes (29) and the vesicular secretion of biliary L and Ch into bile (30), possibly by a microtubule-dependent mechanism (31). Although BS concentrations do not exceed their CMCs within hepatocytes (23, 24), the present work shows that submicellar TCDC preferentially interacts with SUVs composed of the least hydrophobic Ls (Fig. 4), raising the possibility that subselectionof biliary L occurs as BS interact with hepatocyte membranes. Because the influence of L species on micellar TCDC dissolution rates of MLV (Fig. 2) paralleled interaction kinetics of submicellar TCDC-SUV interactions (Figs. 4 and 6), we used these rates to model native biliary L compositions. Assuming that the inverse of $T_{1/2}$ $(T_{1/2})^{-1}$, which represents individual MLV dissolution rates, is proportional to steady state L secretion rates into bile, the molar percentage of each L species was calculated by (16):

$$\%L_i = \frac{(T_{1/2})_i^{-1}}{\sum_i (T_{1/2})_i^{-1}} \qquad Eq.\ 1$$

where i represents the ith L species. This model is clearly simplistic in that it assumes the highly unlikely in vivo possibility of distinct hepatocyte membranes containing individiual L species equally available to the BS. However, we will now demonstrate that the good agreement between our "first order" approximation and the L composition of human bile implicates the role of preferential physical-chemical interactions of BS and hepatocyte membranes in the subselection of biliary L.

Fig. 8 displays the results of these calculations for the six synthetic L species, all as functions of vesicle Ch/L ratio. In the absence of Ch as well as at a Ch/L molar ratio of 0.1, the predicted L compositions (Fig. 8) compare well with that of human hepatic bile (32). These Ch/L ratios

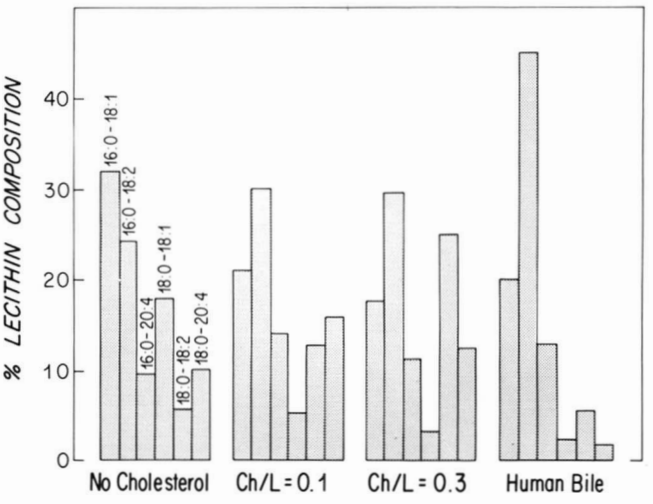

Fig. 8. Predicted biliary L compositions of "bile" based on individual MLV dissolution rates of pure Ls by micellar TCDC. Results are shown for L alone (no Ch) and Ch/L molar ratios of 0.1 and 0.3. The analytical percent composition of L molecular species in human hepatic bile is shown on the right (ref 1, see text for details).

approximate the Ch content of the smooth endoplasmic reticulum (33), which is, in part, believed to be the origin of biliary L and Ch (34) and of the Golgi membranes (33) which are probably involved in membrane lipid traffic destined for bile (35). Our calculations further show that, as the Ch/L ratio was increased to 0.3 (Fig. 8), the predicted proportions of 16:0-20:4 L and 18:0-20:4 L also increased. These lines of in vitro evidence, based on the BS dissolution rates of pure L molecular species and not membrane mixtures, suggest that *1*) BS subselection of the least hydrophobic L for bile could, in part, occur via preferential physical-chemical interactions with hepatocyte smooth endoplasmic reticulum or other membranes; and *2*) if intracellular membrane Ch is increased in the lithogenic state, this might make more arachidonyl L available for BS elution into bile, since this L would be less condensed by Ch in membranes than other L species.

Physical-chemical states of biliary lipids at high dilution

The BS-L-H_2O and BS-L-Ch phase diagrams are important reference frameworks for biliary lipid aggregation during bile formation. The physiologically relevant fragment of the triangular phase diagram in **Fig. 9** demonstrates the equilibrium phase relations of the TCDC-egg yolk L-H_2O system. This is plotted both as moles percentages and weight percentages to facilitate comparisons with similar phase diagrams detailed elsewhere (3, 36, 37), and after which this phase diagram is patterned.[6] Whereas the original phase diagram of Cabral and Small, recently updated (37), was defined for the BS-Na cholate-egg yolk L-water system, we have used the common physiological

bile salt, TCDC. Although the lower CMC of TCDC alters the absolute locations of the phase boundaries, we have assumed that, with TCDC, neither their existence nor their relative configurations are changed appreciably. As inferred from micellar solubility studies, variations in unsaturated L species probably do not significantly alter these phase relations (38), so that the phase relations of egg yolk L (Fig. 9) are likely to be applicable to the pure molecular species studied in this work. The actual phase boundaries have been implicitly derived from our QLS and gel filtration results using egg yolk L and TCDC in the present experiments.

The point on the percent TCDC axis at which the phase boundaries converge represents the CMC of TCDC in 0.15 M NaCl (18). Compositions within the unshaded region comprise the one-phase micellar zone. Intermediate lightly shaded areas form phase regions demarcated by two narrow zones. Both the prototype phase diagram (for Na cholate) (36, 37) and the phase rule dictate that the upper shaded region is composed of two phases, portions of the hexagonal phase coexisting with mixed micelles. The adjoining three-phase region contains a hexagonal phase, a lamellar liquid crystalline phase, and aqueous BS monomers at the CMC (37). Because of the low lipid concentrations in this portion of the phase diagram, the structures of some of these phases remain, as yet, poorly defined. However, from a large body of other work (39–41), compositions falling in the lower two-phase region (heavily shaded area) spontaneously form unilamellar liquid–crystalline vesicles that coexist with BS monomers below their CMC values (39).

Since biliary lipids are concentrated during passage through the biliary tree, the total lipid composition of bile is portrayed by the arrowed line on the phase diagram, labeled "theoretical bile formation path." Since this path crosses all phase boundaries, the physical state of bile, during its lipid concentration, should enter and then exit each of these phase regions in sequence. That is, bile should sequentially contain lamellar liquid–crystalline vesicles, an intermediate hexagonal phase (presumably dispersed as rods), and mixed micelles.

In the present studies, we have tested this hypothesis by studying model bile compositions that fell along a slight modification of the "theoretical bile formation path" (Fig. 9), labeled "experimental bile formation path," with a constant L concentration (2.0 mM). This was chosen to avoid experimental difficulties that would be caused by very low signal-to-noise ratios from highly dilute lipid systems if the theoretical bile formation path were followed (see footnote 5). The relative lipid compositions studied are plotted as open symbols on the experimental bile formation path.

Fig. 10 summarizes the $\overline{R}_h$ values of equilibrated lipid mixtures formed following interactions of egg yolk L SUVs with various TCDC concentrations, i.e., falling along the "experimental bile formation path" in Fig. 9. Since bile dilution is effectively a reversal of bile formation, the shape of this curve is reminiscent of the $\overline{R}_h$ values obtained when a mixed micellar solution is diluted with water (39–41). In addition, similar results have been achieved by dilution of model mixed micellar systems of L with other BS species (39, 40), native dog bile (41), and even with the nonionic detergent, octyl glucoside (42). The designated phase zones in Fig. 10 are derived from the phase diagram in Fig. 9 and depend upon the precision of the CMC of TCDC (18).

Compositions containing submicellar TCDC concentrations (<2 mM) in Fig. 10 fall within a two-phase region (Fig. 9) where lamellar liquid–crystalline vesicles and aqueous BS monomers coexist (36, 39). We observed that

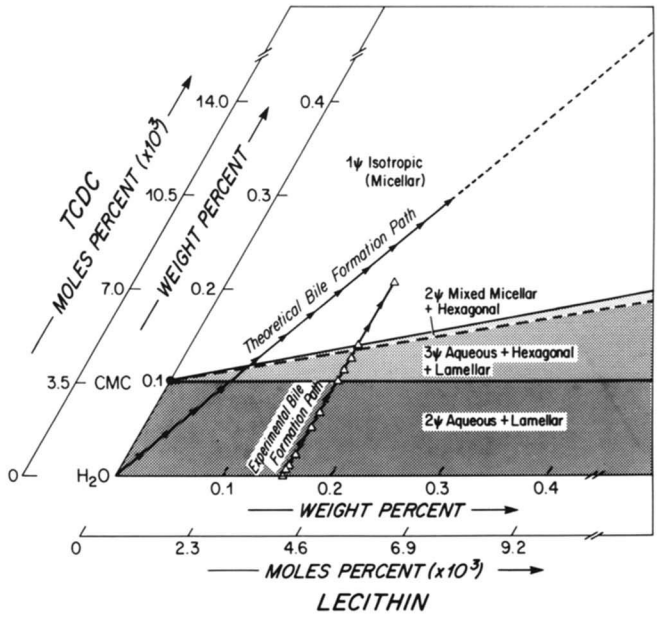

Fig. 9. Fragment of sodium taurochenodeoxycholate (TCDC)-egg yolk L-H_2O triangular phase diagram at high dilution with axes plotted in weights as well as moles percent [6] (pH 7.0, 37°C, 0.15 M NaCl, 5.0 mM Tris-HCl, 1 atm). Solid lines represent precisely defined phase boundaries, whereas the dashed line represents a phase boundary that is not well defined. The phase boundaries and the various phase regions enclosed are the same as for the Na cholate-L-H_2O system (36, 37); however, due to the lower CMC of TCDC (approx. 0.1% or 2 mM), the absolute locations of these boundaries are substantially closer to the base axis of the triangle. The experimental bile formation path defines the compositions of model biles used in this study. For comparison, a theoretical bile formation path is also represented schematically (see text for further discussion).

[6]Two sets of axes are presented in Fig. 9 so that compositions may be determined graphically for both weight and moles percent of TCDC, L, and water. For any composition, weight percent of a component may also be converted mathematically to moles percent. For example: moles percent L = (weight percent wt L/mol · wt L)/(weight percent L/mol · wt L + weight percent TCDC/mol · wt TCDC + weight percent water/mol · wt water). Because moles percent water is intrinsic to these calculations, the CMC of TCDC (2 mM) on the left axis is expressed as 3.5 mol % ($\times 10^3$).

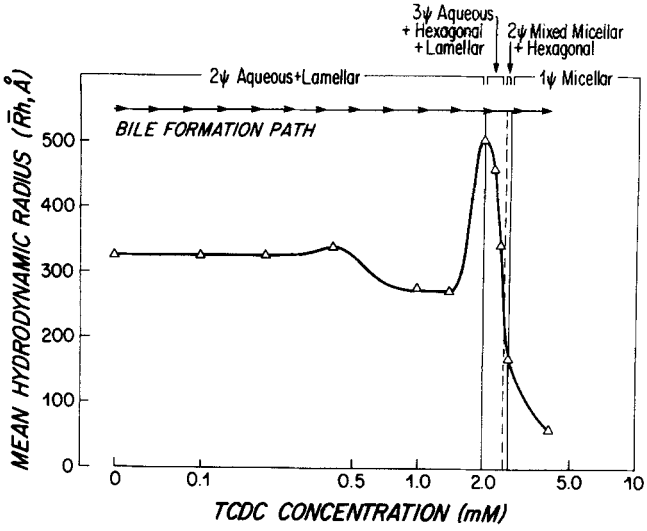

Fig. 10. Dependence of experimental mean hydrodynamic radii ($\bar{R}_h$, Å) on TCDC concentrations for model bile compositions at equilibrium falling along "experimental bile formation path" in Fig. 9 (see text for details). Phase boundaries are plotted as solid and dashed lines. Greek letter ψ represents phase.

most submicellar TCDC (approximately 70 to 80%) became bound to the SUVs; this agrees with literature observations that monomeric BS penetrate model membranes without disrupting overall lipid bilayer integrity (43). The profound decrease in membrane order that occurs when monomeric BS and L interact (44) may explain the transient size increases of SUVs observed upon the addition of 0.4 mM TCDC (Fig. 4A). It is possible that reverse micelle formation within the hydrophobic environment of the bilayers (45) may result in a return to the initial $\bar{R}_h$ values (Fig. 4A and 10) since such micellar packing might have less perturbing effects on the L bilayer structures. Nevertheless, we cannot rule out that these transient size changes may result from osmotic shifts between the core and exterior of SUVs that occur when bilayer permeability increases with BS penetration. Because no change was detected in the SUV-TCDC gel elution profiles at equilibrium (Fig. 5A), submicellar BS concentrations in this range do not appear to alter greatly equilibrium SUV sizes or structure (Fig. 10).

At somewhat higher, but still submicellar, TCDC concentrations (1.0–1.4 mM), BS-induced restructuring of the SUVs was associated with appreciable decreases in $\bar{R}_h$ values (Fig. 4B, upper panel; Fig. 10) and the SUV populations became homogeneous (Fig. 5B). The decreases in V values that occurred during the first 2–3 min after addition of TCDC (Fig. 4B, lower panel) was accompanied by elimination of the small peak that eluted in the void volume. In this connection, Nichols (46) has demonstrated that submicellar BS concentrations greatly enhance monomeric L exchange between unilamellar vesicles; presumably, in our experiments, homogenization of the two SUV populations (Fig. 5A) occurred by this means (Fig. 5B). It is most likely, therefore, that this restructuring induced a fall in $\bar{R}_h$ values in the pre-micellar zone (aqueous plus lamellar phases) in Fig. 10 that would not have occurred if the initial SUV population were monodisperse (Fig. 5A).

As plotted in Fig. 9, concentrations of TCDC just at or slightly above its CMC (2.0 mM) fell in the two- and three-phase regions of the phase diagram that contained a hexagonal phase. The time-dependent $\bar{R}_h$ values of these systems uniformly peaked over a narrow TCDC concentration range and then fell again (Fig. 10). The persistent increase in $\bar{R}_h$ values after addition of 2.0 mM (~CMC) TCDC (Fig. 4C) and the transient increase in $\bar{R}_h$ values at 4 mM TCDC in Fig. 4D are consistent with, but do not prove, formation of dispersed fragments of the hexagonal phase. As demonstrated in Fig. 4C (lower panel), the unusually low V values strongly indicate that the contribution of the largest particles to the intensity of scattered light was so great as to completely dominate the $\bar{R}_h$ measurements (16). Gel filtration of this system at equilibrium demonstrated the presence of two particle populations (Fig. 5C), the larger of which had an $\bar{R}_h$ value of 500 Å and eluted at V_o consistent with fragments of the hexagonal phase. The coexisting smaller aggregates (~ 100 Å in Stokes' radius) had a size range consistent with SUVs; hence, the presence of two particle populations plus aqueous monomeric TCDC (as revealed by ultracentrifugation, see Results) strongly suggests that the overall relative lipid composition of the original mixture fell within the three-phase region of the phase diagram that contained hexagonal, lamellar, and aqueous TCDC phases (Fig. 9 and 10).

That an essentially identical curve is obtained upon serial dilution of a TC-egg L-mixed micellar system (40) suggests that nonmicellar, nonvesicle particles occur within the so-called "vesicle-to-micelle transition." Schurtenberger, Mazer, and Känzig (39) demonstrated that dilution of large BS-L aggregates ($\bar{R}_h$ values ~500 Å) that formed by dilution of BS-L mixed micelles did not alter the $\bar{R}_h$ values of these large aggregates. However, when these authors diluted BS-L mixed micelles to achieve the same final total lipid concentration in a single step, they observed the formation of unilamellar vesicles with $\bar{R}_h$ values of ~200 Å. A reinterpretation of these results suggests that, in the former experiment, the authors diluted a system containing fragments of both the hexagonal phase and SUVs. Upon dilution, as BS migrated to maintain the aqueous phase monomers, the hexagonal phase was most likely transformed into large unilamellar vesicles that coexisted with SUVs. However, we believe that SUvs remained undetected by QLS in these studies due to the disproportionate amount of light scattered by the larger aggregates (16). In our experiments two particle populations of identical proportions always separated both with and without column preequilibration

and elution with the intervesicular TCDC concentration (Fig. 5 C). This suggests that, although the lipid aggregates were diluted approximately 50-fold during gel filtration, no change in particle sizes occurred, even in the absence of the intervesicular TCDC concentration, in agreement with the findings of Schurtengerger et al. (39). Yet, when mixed BS-L micelles were diluted to form SUVs directly (39), our experiments suggest that the hexagonal phase represents a transient intermediate phase (see Fig. 10) that precedes and possibly facilitates SUV formation but does not necessarily persist.

The structure and shape of these presumed fragments of the hexagonal phase in highly dilute systems are presently unknown. With high total lipid concentrations falling within the one-phase hexagonal region at the Na cholate-egg yolk L-H_2O phase diagram, X-ray diffraction reflections are consistent with close-packed, infinitely long, hexagonally packed rods (3). The molecular arrangement of BS and L within these structures is not known but could form via either stacked "mixed disk" micelles (37) or a cylinder composed of BS and L with the acyl chains of the latter in a continuum, possibly oriented toward the center of the cylinders (44). Recently, Hjelm, Thiyagarajan, and Alkam (47) used small angle neutron scattering to study the particle morphology formed upon dilution of glycocholate-L systems essentially identical to those examined by Schurtenberger and coworkers (39) and following a reversal of the bile formation path in Fig. 10. The results suggest that the steep upslope of "micellar" particles and the large peak (Fig. 10) formed upon dilution of mixed micelles are, indeed,elongated rods with a cross-sectional radius of ~ 54 Å.

Higher dilutions of the total lipid concentration yielded SUVs, in agreement with the present work and many other studies (39–41). During the micelle-to-vesicle "transition" upon dilution of BS-L systems, Fromherz and Ruppel (48) demonstrated, by negative stain electron microscopy, the formation of rod-like structures, 200 Å in diameter and ~ 500 Å long, composed of stacked disks with a single bilayer periodicity of 33 Å, strongly suggesting that they did not consist of stacks of flattened vesicles that would have 2 × bilayer periodicity. By replotting the relative compositions of their rod-forming mixtures, we found that the relative BS-L-H_2O composition fell within the dilute three-phase aqueous-plus-hexagonal lamellar zone of the phase diagram (Fig. 10). Similarly, by freeze fracture electron microscopy of model biles, Schubert and coworkers (49) observed "cochleate" cylindrical structures approximately 700 Å in diameter and of undetermined length. Their system contained 3.7 mM Na cholate (approximately the CMC in 0.15 M NaCl 25°C) (45) and 0.75 mM egg L. This relative composition also places the "cochleate" mixtures within the hexagonal-lamellar-aqueous three-phase region of the ternary Na cholate-L-H_2O phase diagram (37, 38), provided the phase boundaries are adjusted downwards for the lower CMC of cholate in 0.15 M NaCl. Our reinterpretation of all of these studies supports the concept that the hexagonal phase containing rods of finite length is found within a very narrow zone of compositions between SUVs and mixed micelles of BS-L-H_2O systems, i.e., between 2.0 and 2.7 mM TCDC in the present work (Fig. 10).

A hexagonal phase, intermediate in micelle formation from TCDC-SUV interactions, was further suggested in the present work when a micellar concentration of 4.0 mM TCDC was added to SUVs. The immediate sharp increase in $\overline{R}_h$ values, declining in size over the next 5 min to that of mixed micelles (Fig. 4D), was most likely due to the transient formation of rods of the hexagonal phase followed by their dissolution into mixed micelles. BS in excess of their CMC will solubilize L bilayers completely as mixed micelles (50) only when the relative lipid composition falls within the micellar zone of an appropriate phase diagram, the size of which varies dramatically with total lipid concentration and BS species (4). As the final lipid composition of the mixture in Fig. 4D does indeed fall inside the respective micellar zone (4) and gel filtration of this system at equilibrium (Fig. 5D) confirms the presence of mixed micelles only, the sharp increase and then decline in $\overline{R}_h$ values are likely due to an SUV-hexagonal-mixed micellar phase sequence. Further, the time-dependent variations in V values for this system (Fig. 4D, lower panel) are most likely related, in that during the micellar dissolution process, varying proportions of SUVs, the hexagonal phase, and mixed micelles coexist (16). In fact, based on turbidimetry, an intermediate hexagonal phase may also occur during L vesicle dissolution by straight-chain nonionic detergent octyl glucoside (42).

Influence of Ch on the physical-chemical states of biliary lipids at high dilution

Although the dilute TCDC-egg L-Ch phase diagram (**Fig. 11**) is not known in detail, the time-dependent variations in $\overline{R}_h$ and V values for TCDC-SUV interactions with Ch/L ratios of 0.33–1.0 revealed that, as TCDC concentrations were increased from below its CMC to 4.0 mM, the structural alterations noted in the absence of Ch (Fig. 4) were progressively eliminated. While this effect was qualitatively consistent with published observations (51) that Ch stabilizes L bilayers to BS penetration and prevents increases in SUV permeability, a phase analysis (not displayed) reveals that, even at the lowest Ch/L ratio, the absolute concentrations (2.0 mM L, 0.67 mM Ch) of the SUV lipids with 4 mM TCDC gave 10.0 moles % Ch, which plotted well outside the micellar zone. No pure micellar phase ever formed.

Nevertheless, a pure micellar phase did form with 8.0 mM TCDC and, on the relevant TCDC-L-Ch phase diagram (Fig. 11), we plot the relative lipid compositions stud-

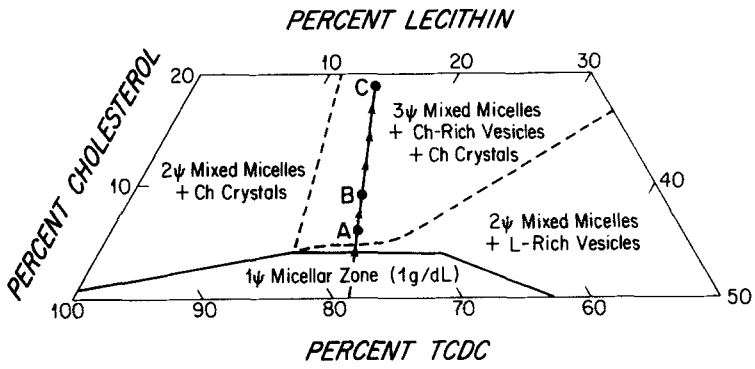

Fig. 11. TCDC-egg yolk L-Ch phase diagram with axes plotted in moles percent (conditions were pH 7.0, 37°C, 0.15 M NaCl, 5.0 mM Tris HCl, 1 atm). Labeled dots represent the overall relative lipid compositions of SUVs composed of 2.0 mM L and variable Ch [Ch/L = (A) 0.33, (B) 0.50, and (C) 1.0] after addition of 8.0 mM TCDC. Solid lines represent experimental phase boundaries, whereas the dashed phase boundaries represent the poorly defined divisions between a three-phase region in the center from two two-phase regions on each side.

ied in Fig. 6 for L-Ch SUVs (Ch/L = (A) 0.33, (B) 0.5, and (C) 1.0), all containing 2.0 mM L and 8.0 mM TCDC. All three relative compositions plotted outside the micellar zone (4) within a three-phase region of the phase diagram where, at equilibrium, Ch-saturated mixed micelles, Ch-L vesicles with a Ch/L ratio of 1.0, and Ch monohydrate crystals should coexist (36). For an interpretation of the data in Fig. 6A, **Fig. 12** schematically depicts the physical-chemical events that likely occur upon addition of 8.0 mM TCDC to SUVs with a Ch/L molar ratio of 0.33 (point A in Fig. 11). The initial increase in $\overline{R}_h$ values (see Fig. 6) is consistent with the formation of a hexagonal rod phase with $\overline{R}_h$ values of 500 Å, followed by a decrease in sizes to $\overline{R}_h$ values of 50 Å due to the progressive dissolution of this phase into mixed micelles. A comparison of the rates of these events with the time-dependent interactions of 4 mM TCDC and SUVs containing no Ch (Fig. 4D, upper panel) indicates that Ch substantially retards TCDC-SUV interactions. The increases in $\overline{R}_h$ values that occur over the next several hundred minutes (Fig. 6 and 12) are consistent with the formation of a new population of vesicles from supersaturated mixed micelles (16, 50). Further, two-component QLS analysis supports this conclusion since the sizes and concentrations of mixed micelles and vesicles are consistent with observations in similar model systems where Ch, in excess of the equilibrium micellar capacity, was incorporated into supersaturated mixed micelles by heating followed by rapid cooling (4, 5). The appearance of a transient population of supersaturated mixed micelles likely derives from the ability of BS to solubilize larger amounts of L more rapidly than Ch since, at equilibrium, the relative composition at point A (Fig. 11) is only ~50% saturated with L but supersaturated with Ch. The formation of a new population of vesicles from supersaturated mixed micelles likely represents the precipitation of Ch-rich particles. As described in studies of Ch nucleation in model bile systems (5), the L contained in these particles serves to minimize the interfacial energy of Ch in this metastable system. As shown in Fig. 6B, the time-dependent changes in $\overline{R}_h$ values at a Ch/L ratio of 0.5 (point B, Fig. 12) probably represent similar events, although the transitions are temporally and kinetically obscured by the higher Ch content. In the system with a Ch/L ratio of 1.0, the SUVs were resistant to complete dissolution into mixed micelles by TCDC and, in fact, as inferred by QLS, no further change occurred following an abrupt increase in $\overline{R}_h$ values (Fig. 6C). Nevertheless, as demonstrated in Fig. 7, TCDC enacted dramatic changes for this (Ch/L = 1.0) system; TCDC micelles remodeled the SUVs, presumably by extracting and solubilizing greater amounts of L than

Fig. 12. Schematic representation of the putative molecular events after addition of 8.0 mM TCDC with SUVs composed of 2.0 mM 16:0–18:1 L with Ch in a molar ratio of Ch/L = 0.33 (actual data are redrawn from Fig. 6A; interpretation and discussion are based on the $\overline{R}_h$ values, V values, and the phase equilibria considerations in this paper). The fine structure of the putative hexagonal rod phase is not known, but is shown schematically as stacked discs.

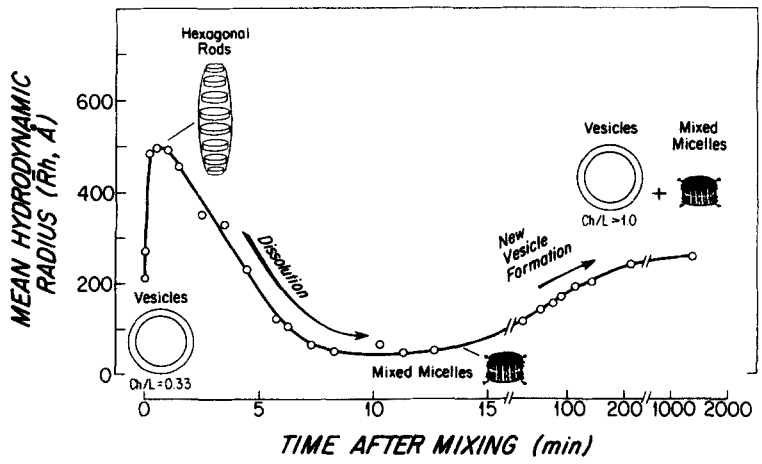

Ch, to form saturated mixed micelles and Ch-enriched SUVs with Ch/L ratios of 2:1 (Fig. 7B). This Ch/L vesicle ratio is identical to that observed by Mazer and Carey (5) in more concentrated systems following heating to form homogeneous micellar phases and then cooling to induce precipitation.

Pathophysiological implications

The observations in model systems provide relevant insights concerning the aggregative states of biliary lipids following their canalicular secretion. They describe the complex physical-chemical pathway to high total lipid concentrations in gallbladder bile. From the hepatocyte to canaliculi, BS are probably secreted in monomeric form and Ch/L molecules are secreted as SUVs (24, 30). Once secreted, BS probably induce SUV aggregation to first form rods of the hexagonal phase as the total lipid concentration rises along the "bile formation path" (Fig. 9). This occurs secondary to water reabsorption in the bile ductules (52) and to the possible existence of BS in perimicellar concentrations within the hepatic canaliculus (24). Although the physical compositions of bile will rapidly traverse this very narrow hexagonal phase-containing region (Fig. 9), the presence of Ch, as we have demonstrated, will greatly retard the dissolution rates of both vesicles (30) and, perhaps, the putative rod-like phase. Therefore, portions of this phase, as well as vesicles (30), may be transient or persist even after most of the total lipid concentration has been dissolved by BS into mixed micelles. Moreover, based upon phase considerations, it is possible that the hexagonal phase may be formed de novo from micellar phase lipids in gallbladder bile. Fluid dynamics analysis suggests that, due to rapid gallbladder absorption of water, solvent drags may induce concentration of the total bile lipid concentration within the juxtamucosal unstirred water layer (53) so that lipid compositions may fall within the region of the phase diagram where the hexagonal phase exists as a single phase zone (3, 36, 37). The persistence or new formation of hexagonal phase rods may explain the observation of "cigar-shaped assemblies" first observed by Howell et al. (54) in concentrated native and model gallbladder biles two decades ago.

Supported in part by Grant Nos. DK36588, DK34854, and GM07258 from the National Institutes of Health (U.S. Public Health Service), and a NATO grant (#0078/86) for international collaboration in research. D. E. C. was also supported by Public Health Service National Research Service Award 5T32GM07753-08 from the National Institute of General Medical Science. We are most grateful to Dr. Michael A. O'Donovan for this gift of radiolabeled TCDC and to Ms. Rebecca Ankener for expert editing and word-processing of this manuscript.

Manuscript received 8 May 1989 and in revised form 29 August 1989.

REFERENCES

1. Cantafora, A., A. Di Biase, D. Alvaro, M. Angelico, M. Marin, and A. F. Attili. 1983. High performance liquid chromatographic analysis of molecular species of phosphatidylcholine. Development of a quantitative assay and its application to human bile. *Clin. Chim. Acta.* **134:** 281–295.
2. Patton, G. M., J. M. Fasulo, and S. J. Robbins. 1982. Separation of phospholipids and individual molecular species of phospholipids by high-performance liquid chromatography. *J. Lipid Res.* **23:** 190–196.
3. Small, D. M., M. Bourgès, and D. G. Dervichian. 1966. Ternary and quarternary aqueous systems containing bile salts, lecithin and cholesterol. *Nature.* **211:** 816–820.
4. Carey, M. C., and D. M. Small. 1978. Physical chemistry of cholesterol solubility in bile. Relationships to gallstone formation and dissolution in man. *J. Clin. Invest.* **61:** 998–1026.
5. Mazer, N. A., and M. C. Carey. 1983. Quasielastic light scattering studies of aqueous biliary lipid systems. Cholesterol solubilization and precipitation in model bile systems. *Biochemistry.* **22:** 426–442.
6. Sömjen, G. T., and T. Gilat. 1983. A non-micellar mode of cholesterol transport in human bile. *FEBS Lett.* **156:** 265–268.
7. Carey, M. C., and M. J. Cahalane. 1988. Enterohepatic circulation. *In* The Liver: Biology and Pathobiology. I. M. Arias, W. B. Jacoby, H. Popper, D. Schacter, and D. A. Shafritz, editors. Second edition. Raven Press, New York. 573–616.
8. O'Donovan, M. A. 1986. Hepatic bile salt metabolism: studies in the isolated perfused rat liver. M. D. Thesis. National University of Ireland, Dublin, Ireland. 1–270.
9. Bangham, A. D., M. W. Hill, and N. G. A. Miller. 1974. Preparation and use of liposomes as models of biological membranes. *In* Methods in Membrane Biology. E. D. Korn, editor. Plenum Press, New York. 1–68.
10. Hauser, H., and L. Irons. 1972. The effect of ultrasonication on the chemical and physical properties of egg yolk lecithin dispersions. *Z. Physiol. Chem.* **353:** 1579–1590.
11. Klein, R. A. 1970. The detection of oxidation in liposomes preparations. *Biochim. Biophys. Acta.* **210:** 486–489.
12. Huang, C. 1969. Studies on phosphatidylcholine vesicles. Formation and physical characteristics. Biochemistry. **8:** 344–351.
13. Goll, J., F. D. Carlson, Y. Barenholz, B. J. Litman, and T. E. Thompson. 1982. Photon correlation spectroscopy study of the size distribution of phospholipid vesicles. *Biophys. J.* **38:** 7–13.
14. Lentz, B. R., T. J. Carpenter, and D. R. Alford. 1987. Spontaneous fusion of phosphatidylcholine small unilamellar vesicles in the fluid phase. *Biochemistry.* **26:** 5389–5397.
15. Lichtenberg, D., Y. Zilberman, P. Greenzaid, and S. Zamir. 1979. Structural and kinetic studies on the solubilization of lecithin by sodium deoxycholate. *Biochemistry.* **18:** 3517–3525.
16. Cohen, D. E. 1986. Studies of biliary lipid secretion in model and native biles. Ph.D. Dissertation, Harvard University, Cambridge, MA. 1–207.
17. Koppel, D. E. 1972. Analysis of macromolecular polydispersity in intensity correlation spectroscopy: the method of cumulants. *J. Chem. Phys.* **57:** 4814–4820.
18. Carey, M. C., J. C. Montet, M. C. Phillips, M. J. Armstrong, and N. A. Mazer. 1981. Thermodynamic and molecular basis for dissimilar cholesterol solubilizing capacities by micellar solutions of bile salts: cases of sodium chenodeoxycholate and sodium ursodeoxycholate and their glycine and taurine conjugates. *Biochemistry.* **20:** 3637–3648.
19. Gurantz, D., F. Laker, and A. F. Hofmann. 1981. Enzymatic measurement of choline-containing phospholipids in bile. *J. Lipid Res.* **22:** 373–376.

20. Kern, F., Jr., H. Eriksson, T. Curstedt, and J. Sjövall. 1977. Effect of ethynylestradiol on biliary excretion of bile acids, phosphatidylcholines, and cholesterol in the bile fistula rat. *J. Lipid Res.* **18:** 623–634.
21. Rajagopalan, N., and S. Lindenbaum. 1984. Kinetics and thermodynamics of the formation of mixed micelles of egg phosphatidylcholine and bile salts. *J. Lipid Res.* **25:** 135–147.
22. Scherstén, T., S. Nilsson, E. Cahlin, M. Filipson, and G. Brodin-Persson. 1971. Relationship between the biliary excretion of bile acids and the excretion of water, lecithin and cholesterol in man. *Eur. J. Clin. Invest.* **1:** 242–247.
23. Simion, F. A., B. Fleischer, and S. Fleischer. 1984. Subcellular distribution of bile acids, bile salts, and taurocholate binding in rat liver. *Biochemistry.* **23:** 6459–6466.
24. Frimmer, M., and K. Ziegler. 1988. The transport of bile acids in liver cells. *Biochim. Biophys. Acta.* **947:** 75–99.
25. Middelkoop, E., B. H. Lubin, J. A. F. Op den Kamp, and B. Roelofsen. 1986. Flip-flop rates of individual molecular species of phosphatidycholine in the human red cell membrane. *Biochim. Biophys. Acta.* **855:** 421–424.
26. Patton, G. M., S. J. Robins, J. M. Fasulo, and S. Bennett Clark. 1985. Influence of lecithin acyl chain composition on the kinetics of exchange between chylomicrons and high density lipoproteins. *J. Lipid Res.* **26:** 1285–1293.
27. Coolbear, K. P., C. B. Berde, and K. M. W. Keough. 1983. Gel to liquid-crystalline phase transitions of aqueous dispersions of polyunsaturated mixed acid-phosphatidylcholines. *Biochemistry.* **22:** 1466–1473.
28. Guyer, W., and K. Bloch. 1983. Phosphatidylcholine and cholesterol interactions in model membranes. *Chem. Phys. Lipids.* **33:** 313–322.
29. Jones, A. L., D. L. Schmucker, J. S. Mooney, R. K. Ockner, and R. D. Adler. 1979. Alterations in hepatic pericanalicular cytoplasm during enhanced bile secretory activity. *Lab Invest.* **40:** 512–517.
30. Cohen, D. E., M. Angelico, and M. C. Carey. 1989. Quasi-elastic light scattering evidence for vesicular secretion of biliary lipids. *Am. J. Physiol.* **257:** G1–G8.
31. Barnwell, S. G., P. J. Lowe, and R. Coleman. 1984. The effects of colchicine on secretion into bile of bile salts, phospholipids, cholesterol and plasma membrane enzymes: bile salts are secreted unaccompanied by phospholipid and cholesterol. *Biochem. J.* **220:** 723–731.
32. Angelico, M., D. Alvaro, A. F. Atilli, and A. Cantafora. 1985. Mechanisms of secretion of biliary phosphatidylcholes: the role of bile acids. *Ital. J. Gastroenterol.* **17:** 278–281.
33. Zambrano, F., S. Fleischer, and B. Fleischer. 1975. Lipid composition of the Golgi apparatus of rat kidney and liver in comparison with other subcellular organelles. *Biochim. Biophys. Acta.* **380:** 357–369.
34. Gregory, D. H., Z. R. Valchevic, P. Schatzki, and L. Swell. 1975. MEchanism of secretion of biliary lipids I. Role of bile canalicular and microsomal membranes in the synthesis and transport of biliary lecithin and cholesterol. *J. Clin. Invest.* **55:** 105–114.
35. Lamri, Y., A. Roda, M. Dumont, G. Feldman, and S. Erlinger. 1988. Immunoperoxidase localization of bile salts in rat liver cells. Evidence for a role of the Golgi apparatus in bile salt transport. *J. Clin. Invest.* **82:** 1173–1182.
36. Carey, M. C. 1988. Lipid solubilization in bile. *In* Bile Acids in Health and Disease. T. C. Northfield, R. P. Jazrawi, and P. L. Zantler-Munro, editors. Kluwer Academic, Dordrecht, Germany. 61–82.
37. Cabral, D. J., and D. M. Small. 1990. The physical chemistry. of bile. *In* Handbook of Physiology. J. G. Forte, editor. American Physiology Society, Washington, DC. In press.
38. Saunders, D. R., and M. A. Wells. 1969. The cholesterol solubilizing capacity of lecithins in aqueous solutions of bile salt. *Biochim. Biophys. Acta.* **76:** 828–835.
39. Schurtenberger, P., N. Mazer, and W. Känzig. 1985. Micelle to vesicle transition in aqueous solutions of bile salt and lecithin. *J. Phys. Chem.* **89:** 1042–1049.
40. Donovan, J. M., G. B. Benedek, and M. C. Carey. 1987. Formation of mixed micelles and vesicles of human apolipoproteins A-I and A-II with synthetic and natural lecithins and the bile salt taurocholate: quasielastic light scattering studies. *Biochemistry.* **26:** 8125–8133.
41. Mazer, N. A., P. Schurtenberger, M. C. Carey, R. Preisig, K. Weigand, and W. Känkig. 1984. Quasi-elastic light scattering studies of native hepatic bile from the dog: comparison with aggregative behavior of model biliary lipid systems. *Biochemistry.* **23:** 1994–2005.
42. Ollivon, M., O. Eidelman, R. Blumenthal, and A. Walter. 1988. Micelle-vesicle transition of egg phosphatidylcholine and octyl glucoside. *Biochemistry.* **27:** 1695–1703.
43. Saitô, H., Y. Sugimoto, R. Tabeta, S. Suzuki, G. Izumi, M. Kodama, S. Toyoshima, and C. Nagata. 1983. Incorporation of bile acid of low concentration into model and biological membranes studied by ^{2}H and ^{31}P NMR. *J. Biochem.* **94:** 1877–1887.
44. Ulmius, J., G. Lindblöm, H. Wennerström, L. B-A. Johansson, K. Fontell, O. Soderman, and G. Arvidson. 1982. Molecular organization in the liquid crystalline phases of lecithin–sodium cholate–water systems studied by nuclear magnetic resonance. *Biochemistry.* **21:** 1553–1560.
45. Carey, M. C. 1985. Physical chemical properties of bile acids and their salts. *In* New Comprehensive Biochemistry. Vol. 12. J. Sjövall and H. Danielson, editors. Elsevier, Amsterdam. 345–403.
46. Nichols, J. W. 1986. Low concentrations of bile salts increase the rate of spontaneous phospholipid transfer between vesicles. *Biochemistry.* **25:** 4596–4601.
47. Hjelm, R. P., Jr., P. Thiyagarajan, and H. Alkan. 1988. A small-angle neutron scattering study of the effects of dilution on particle morphology in mixtures of glycocholate and lecithin. *J. Appl. Crystallogr.* **21:** 858–863.
48. Fromherz, P., and D. Rüppel. 1985. Lipid vesicle formation: the transition from open disks to closed shells. *FEBS Lett.* **179:** 155–159.
49. Schubert, R., K. Beyer, H. Wolberg, and K. Schmidt. 1986. Structural changes in membranes of large unilamellar vesicles after binding of sodium cholate. *Biochemistry.* **25:** 5263–5269.
50. Lichtenberg, D., S. Ragimova, A. Bor, S. Almog, C. Vinkler, M. Kalina, Y. Peled, and Z. Halpern. 1988. Stability of mixed micellar bile models supersaturated with cholesterol. *Biophys. J.* **54:** 1013–1025.
51. Castellino, F. J., and B. N. Violand. 1979. ^{31}P-Nuclear magnetic resonance and $^{31}P\{^{1}H\}$nuclear Overhauser effect analysis of mixed egg phosphatidylcholine-sodium taurocholate vesicles and micelles. *Arch. Biochem. Biophys.* **193:** 543–550.
52. Tavaloni, N. 1985. Role of ductular water reabsorption in canine bile secretion. *J. Lab. Clin. Med.* **106:** 154–161.
53. Cussler, E. L., D. F. Evans, and R. G. DePalma. 1970. A model for gallbladder function and cholesterol gallstone formation. *Proc. Natl. Acad. Sci. USA.* **67:** 400–407.
54. Howell, J. I., J. A. Lucy, R. C. Pirola, and I. A. D. Bouchier. 1970. Macromolecular assemblies of lipid in bile. *Biochim. Biophys. Acta.* **210:** 1–6.